

Ian R. Winship · Douglas R. W. Wylie

## Responses of neurons in the medial column of the inferior olive in pigeons to translational and rotational optic flowfields

Received: 27 November 2000 / Accepted: 2 July 2001 / Published online: 6 September 2001  
© Springer-Verlag 2001

**Abstract** The responses of neurons in the medial column of the inferior olive to translational and rotational optic flow were recorded from anaesthetized pigeons. Panoramic translational or rotational flowfields were produced by mechanical devices that projected optic flow patterns onto the walls, ceiling and floor of the room. The axis of rotation/translation could be positioned to any orientation in three-dimensional space such that axis tuning could be determined. Each neuron was assigned a vector representing the axis about/along which the animal would rotate/translate to produce the flowfield that elicited maximal modulation. Both translation-sensitive and rotation-sensitive neurons were found. For neurons responsive to translational optic flow, the preferred axis is described with reference to a standard right-handed coordinate system, where  $+x$ ,  $+y$  and  $+z$  represent rightward, upward and forward translation of the animal, respectively (assuming that all recordings were from the right side of the brain).  $t(+y)$  neurons were maximally excited in response to a translational optic flowfield that results from self-translation upward along the vertical ( $y$ ) axis.  $t(-y)$  neurons also responded best to translational optic flow along the vertical axis but showed the opposite direction preference. The two remaining groups,  $t(-x+z)$  and  $t(-x-z)$  neurons, responded best to translational optic flow along horizontal axes that were oriented  $45^\circ$  to the midline. There were two types of neurons responsive to rotational optic flow:  $rVA$  neurons preferred rotation about the vertical axis, and  $rHI35c$  neurons preferred rotation about a horizontal axis at  $135^\circ$  contralateral azimuth. The locations of marking lesions indicated a clear topographical organization of the six response types. In summary, our results rein-

force that the olivo-cerebellar system dedicated to the analysis of optic flow is organized according to a reference frame consisting of three approximately orthogonal axes: the vertical axis, and two horizontal axes oriented  $45^\circ$  to either side the midline. Previous research has shown that the eye muscles, vestibular semicircular canals and postural control system all share a similar spatial frame of reference.

**Keywords** Optokinetic · Inferior olive · Vestibulocerebellum · Visual-vestibular integration · Self-motion · Pigeon

### Introduction

Self-motion of an organism through the environment containing numerous stationary objects and surfaces induces distinctive patterns of visual motion, termed optic flow or “flowfields”, across its entire retina (Gibson 1954). Thus, optic flow provides visual proprioceptive information, which, in conjunction with information from other sensory systems including the vestibular and somatosensory systems, is important for the control of posture and self-motion.

Previous research has shown that the complex spike activity (CSA) of Purkinje cells in the vestibulocerebellum (VbC) of pigeons is modulated in response to particular patterns of optic flow (Wylie and Frost 1991, 1993, 1999a; Wylie et al. 1993, 1998). Neurons in the lateral VbC (flocculus) respond best to rotational flowfields (see Fig. 1b), whereas neurons in the medial VbC (ventral uvula and nodulus) respond to translational flowfields (see Fig. 1c; Wylie et al. 1993). It was originally shown in rabbits, by Simpson, Graf and colleagues (Simpson et al. 1981, 1988a, 1988b; Graf et al. 1988; Leonard et al. 1988), that the flocculus neurons respond best to rotational optic flow about either the vertical axis or a horizontal axis oriented at  $135^\circ$  ipsilateral/ $45^\circ$  contralateral azimuth ( $rVA$  and  $rHI35i$  neurons, respectively). This was confirmed in pigeons (Wylie and Frost

I.R. Winship · D.R.W. Wylie (✉)  
Department of Psychology, University of Alberta, Edmonton,  
Alberta, Canada, T6G 2E9  
e-mail: dwylie@ualberta.ca  
Tel.: +1-780-4925274, Fax: +1-780-4921768

D.R.W. Wylie  
Division of Neuroscience, University of Alberta, Edmonton,  
Alberta, Canada, T6G 2E9

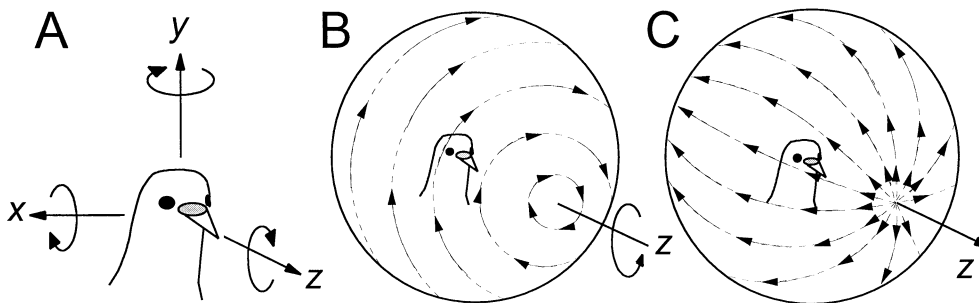


**Fig. 1** **a** The standard coordinate system for motion of an object in three-dimensional space. It is sufficient to describe motion using a reference frame consisting of three orthogonal axes ( $x$ ,  $y$ ,  $z$ ), and 6 degrees of freedom, three of translation and three of rotation. In vision research,  $x$ ,  $y$  and  $z$  represent the interaural, vertical and naso-occipital axes, respectively. With respect to the direction of translation,  $+x$ ,  $+y$  and  $+z$  represent rightward, upward and forward self-motion respectively. **b** The optic flowfield resulting from clockwise head rotation about the  $z$ -axis. The *arrows*, as projected onto a sphere, illustrate the counter-clockwise rotation of local motion in the flowfield, which collectively constitute the wholefield rotational optic flow. **c** A schematic of the optic flowfield resulting from translation along the  $+z$ -axis. At the “pole” in the direction of translation, the *arrows* diverge from a point; the focus of expansion. Likewise, at the opposite pole (not shown) the vectors would converge to a point; the focus of contraction. At the “equators” of the sphere, the flowfield is laminar, with all vectors pointing in approximately the same direction

1993). Simpson and colleagues emphasized that the reference frame of the floccular neurons responsive to rotational optic flow, i.e. the vertical axis and horizontal axes  $45^\circ$  to the midline, is common to the vestibular canals and eye muscles (Graf and Simpson 1981; Simpson and Graf 1981, 1985; Ezure and Graf 1984; Graf et al. 1988; Leonard et al. 1988; Simpson et al. 1988a, 1988b, 1989a, 1989b; van der Steen et al. 1994; see also Wylie and Frost 1996).

CSA responsive to translational optic flow has only been found in the ventral uvula and nodulus of pigeons (Wylie and Frost 1991, 1999a; Wylie et al. 1993, 1998). With respect to the preferred axes of translational optic flow, there are four response types. The orientation of the best axis of translational optic flow for each of the four types is described using the reference frame depicted in Fig. 1a.  $x$ ,  $y$  and  $z$  represent the interaural, vertical and naso-occipital axes, respectively. With respect to direction,  $+x$ ,  $+y$  and  $+z$  represent rightward, upward and forward self-translation, respectively. Neurons respond best to optic flow patterns resulting from either upward or downward self-translation along the vertical axis [ $t(+y)$  and  $t(-y)$  neurons] or self-translation along one of two horizontal axes oriented  $45^\circ$  to the midline [ $t(-x-z)$  and  $t(-x+z)$  neurons, assuming recording from the left VbC; Wylie et al. 1998; Wylie and Frost 1999a. Thus, this three-axes reference frame, the vertical axis and horizontal axes  $45^\circ$  to the midline, is common to both the translational and the rotational optic flow systems.

Previous anatomical research using retrograde transport from the pigeon VbC has shown that the different types of translation- and rotation-sensitive Purkinje cells

receive climbing fibre (CF) input from discrete regions of the contralateral medial column (mc) of the inferior olive (IO; Wylie et al. 1999; Crowder et al. 2000). In this report we investigated the CSA of neurons in the mc in response to translational and rotational optic flowfields.

## Methods

### Surgery

The methods reported herein conformed to the guidelines established by the Canadian Council on Animal Care and were approved by the Biosciences Animal Care and Policy Committee at the University of Alberta. Silver King or Homing pigeons were anaesthetized with a ketamine (65 mg/kg)-xylazine (8 mg/kg) mixture (i.m.), and supplemental doses were administered as necessary. The animals were placed in a stereotaxic device with pigeon ear bars and beak adapter such that the orientation of the skull conformed to the atlas of Karten and Hodos (1967). A section of bone and dura on the right side of the head starting near the midline and extending laterally was then removed to expose the cerebellum.

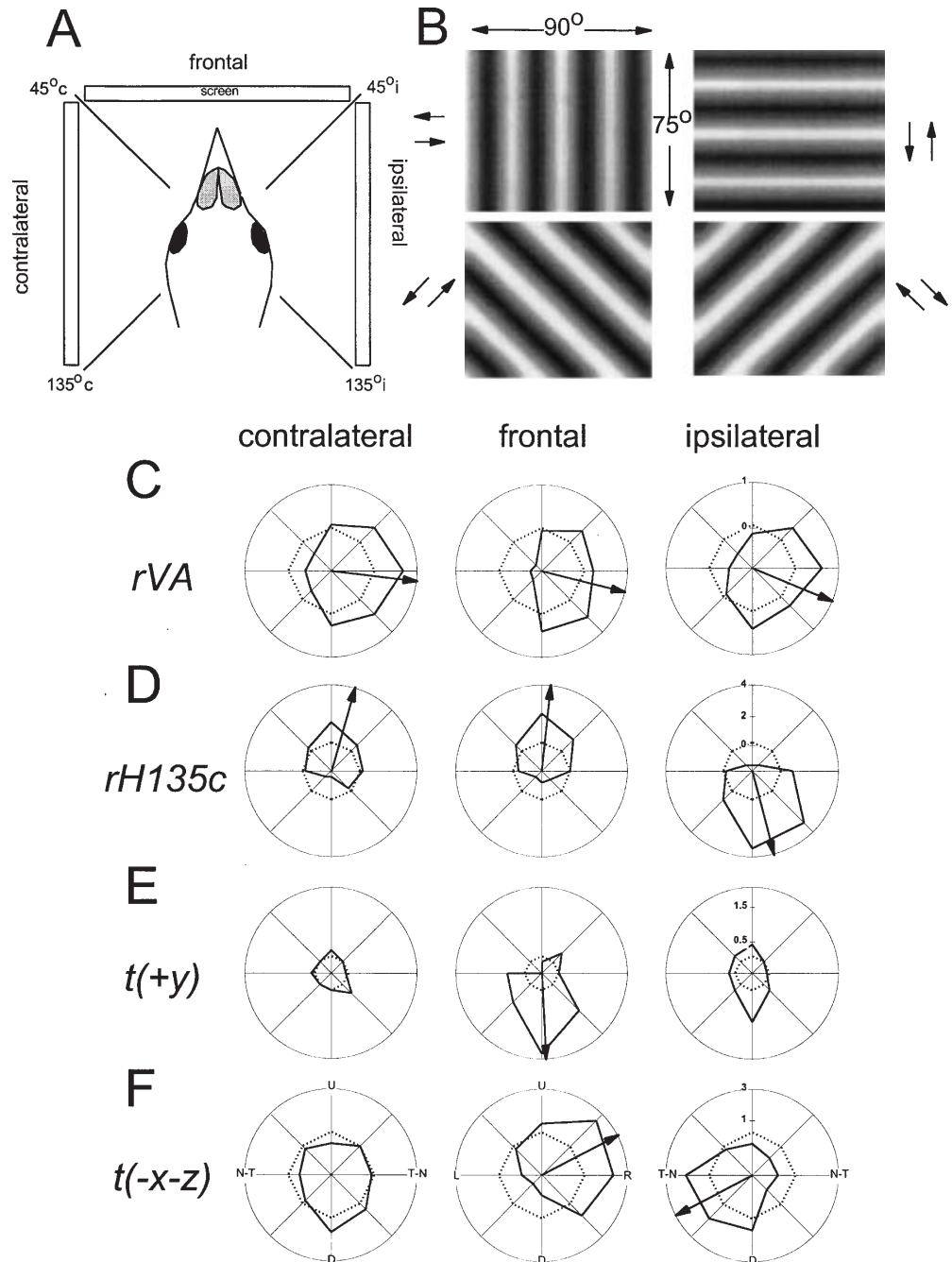
### Extracellular recordings and optic flow stimulation

After exposure of the cerebellum, birds were removed from the ear bars and beak adapter, and their heads were oriented such that their eye-beak angle was  $34^\circ$  (the normal orientation of the head; Erichsen et al. 1989). This involved rotating the beak upward about the inter-aural axis approximately  $38^\circ$  relative to the stereotaxic position of Karten and Hodos (1967). Extracellular recordings were then made with glass micropipettes filled with 2 M NaCl (tip diameters of 3–5  $\mu\text{m}$ ) or tungsten metal electrodes (Frederick Haer). To access the optic flow-sensitive neurons in the mc, the electrode was oriented  $10^\circ$  to the sagittal plane and  $38^\circ$  to the frontal plane to compensate for adjustment of the bird's eye-beak angle. Electrodes were advanced through the nodulus and brainstem using a hydraulic microdrive (Frederick Haer). Extracellular signals were amplified, filtered and fed to a window discriminator, which produced TTL pulses, each representing a single spike time. TTL pulses were fed to a data analysis system (Cambridge Electronic Designs, CED; 1401plus) and peri-stimulus time histograms (PSTHs) were constructed using Spike2 software (CED).

IO cells were identified based on their characteristic firing rate of about 1 spike/s. Once a cell was isolated, it was first stimulated with a large (about  $90^\circ \times 90^\circ$ ), handheld stimulus consisting of a random pattern of dots and lines to determine whether the cell was sensitive to visual stimulation. Generally, by moving this stimulus in different areas of the panoramic binocular visual field, the preferred flowfield can be qualitatively determined. However, because these neurons are broadly tuned for the direction of motion, a computer-generated stimulus was used to confirm the flowfield preference. The procedure is illustrated in Fig. 2. A screen measuring  $90^\circ \times 75^\circ$  (width  $\times$  height) was positioned in one of three locations relative to the bird's head: the frontal visual

**Fig. 2a–f** Response of medial column neurons to moving largefield sine wave gratings presented in different regions of the visual field. Drifting sine wave gratings were back-projected onto the screen that measured  $90^\circ \times 75^\circ$  (width  $\times$  height). **a** The screen was positioned at one of three locations relative to the bird: the contralateral, ipsilateral and frontal regions (assuming recordings were made in the right inferior olive).

**b** shows the four grating orientations used to determine tuning curves in each location. Each grating moved in both directions, perpendicular to the orientation of the grating, to produce a tuning curve with a total of eight directions ( $45^\circ$  increments). **c–f** show responses of *rVA* (**c**), *rH135c* (**d**), *t(+y)* (**e**) and *t(-x-z)* (**f**) neurons to the drifting gratings in each of the three regions. Polar plots of direction tuning are shown (firing rate in spikes per second re. spontaneous rate (SR) as a function of the direction of largefield motion). The *broken circles* represent the SR (set to 0 spikes/s) and the *arrows* represent the peak of the best-fit cosine (i.e. the preferred or “best” direction). Best-fit cosines were only done for those tuning curves that had a modulation index  $\approx 1.5$  (see Results). (*U, D, L, R* Upward, downward, leftward and rightward motion, *N-T, T-N* nasal-to-temporal and temporal-to-nasal motion, *i* ipsilateral, *c* contralateral)



field (from  $45^\circ$  ipsilateral, *i*, to  $45^\circ$  contralateral, *c*, azimuth), the contralateral hemifield (from  $45^\circ$  *c* to  $135^\circ$  *c* azimuth), or the ipsilateral hemifield (from  $45^\circ$  *i* to  $135^\circ$  *i* azimuth; see Fig. 2a). Drifting sine wave gratings (in one of four orientations; illustrated in Fig. 2b) of an effective spatial and temporal frequency were then generated by a VSGThree (Cambridge Research Services) and back-projected (InFocus LP750) onto the screen. Direction tuning curves in each of the three areas of the visual field were obtained by moving the gratings in eight different directions (see Fig. 2b). Responses were averaged over at least 3 sweeps, where each sweep consisted of 5 s of motion in one direction, a 5-s pause, and 5 s of motion in the opposite direction, followed by a 5-s pause. Although this procedure did not elicit maximal modulation of the cell, it was quite useful for identifying the cell type for subsequent testing. (For example, translation-sensitive neu-

rons prefer approximately the same direction of motion in both the ipsi- and contralateral hemifields, whereas rotation neurons prefer the opposite directions of motion in the ipsi- and contralateral hemifields (e.g. Fig. 2c–f).

Rotation-sensitive cells were further studied using a *planetarium* projector (see Wylie and Frost 1993, 1999b). Modelled after that designed by Simpson and colleagues (Simpson et al. 1981), this device consisted of a small, hollow cylinder ( $3 \times 7$  cm, radius  $\times$  height) perforated with numerous small holes, and fixed around a small filament light source. Using a function generator and a pen motor, the cylinder was rotated such that a moving pattern of light dots was projected onto the floors, ceiling and walls of the room. The resultant rotational flowfield covered the entire panoramic visual field except a circular area (about  $60^\circ$  diameter) at the base of the cylinder.

Translation-sensitive neurons were further studied with the *translator* projector (see Wylie and Frost 1999a). Similar to the planetarium projector, the translator consisted of a small, hollow metal sphere (diameter 9 cm), the surface of which was drilled with numerous small holes. A small filament light source was moved along a path within the sphere (under computer control), such that a simulated translational flowfield, (with a focus of expansion, FOE, at one “pole”, a focus of contraction, FOC, at the opposite pole, and laminar flow at the “equator”; see Fig. 1c) was projected onto the walls, ceiling and floor of the room. As with the planetarium, this pattern essentially covered the entire binocular visual field.

For both devices, the dots subtended  $1\text{--}2^\circ$ . For the planetarium the dots rotated in the range of  $1\text{--}2^\circ/\text{s}$ . For the translator, there is a gradient of velocity, with the dots at the poles moving slowest, and the dots along the equator moving the fastest. The “equatorial” dots moved at speeds in the range of  $1\text{--}10^\circ/\text{s}$ . By mounting the planetarium/translator in gimbals, the axis of the rotational/translational flowfield could be positioned to any orientation within three-dimensional space.

Mean firing rates for each axis for were determined from 5 to 15 sweeps. For the planetarium, each sweep consisted of 5 s of rotation in one direction, followed by 5 s of rotation in the opposite direction. For the translator, each sweep consisted of 5 s of motion in one direction along the axis of the translator, a 5-s pause, 5 s of translation in the opposite direction, and a 5-s pause.

Upon completion of physiological recording, in some cases electrolytic marking lesions were made ( $30\ \mu\text{A}$  for 10 s) at known locations relative to recording sites such that the topographical organization of the mc could be determined. These animals were administered an overdose of pentobarbital sodium and immediately perfused with 0.9% saline followed by 4% para-formaldehyde. The brains were extracted and cryoprotected with sucrose. Frozen sections ( $44\ \mu\text{m}$  thick) in the coronal plane were collected and mounted onto gelatin-coated slides. The sections were stained with neutral red and examined using light microscopy.

## Results

The activity of 49 neurons sensitive to optic flow stimuli was recorded from 20 pigeons. The mean spontaneous firing was  $1.53 \pm 0.11$  spikes/s (mean  $\pm$  SEM). These cells responded to large moving visual stimuli and preferred particular patterns of optic flow resulting from either self-translation or self-rotation. The identification of these cells was made relatively easy by examining the responses to drifting largefield sine wave gratings presented to either the frontal, contralateral and ipsilateral visual fields (see Fig. 2). Neurons responsive to rotational optic flow prefer approximately opposite directions of motion in the ipsi- and contralateral visual fields (e.g. Fig. 2b, d), whereas neurons responsive to translational optic flow prefer the same direction of motion in the ipsi- and contralateral visual fields. In response to the panoramic flowfield stimuli produced by the planetarium and translator projectors, neurons showed maximal excitation in response to rotational/translational optic flow about/along a particular axis (“best” or “preferred” axis) and maximal inhibition in response to optic flow in the opposite direction about/along the same axis. Little or no modulation occurred in response to optic flow along/about axes orthogonal to the best axis (“null” axes). A modulation index (MI) was calculated for each neuron by taking the ratio of the firing rates in response to the two directions of optic flow about/along the preferred

axis (max/min). A neuron was deemed optic flow sensitive if the MI was  $\geq 1.5$ . The mean MI for the 49 neurons was 3.27 (range 1.6–10.1). The “axis tuning” was quite broad, and the tuning curves in any particular plane approximated a cosine function. The peak of the best-fit cosine was used to assign the preferred axis for each tuning curve. It is assumed that all recordings were obtained from the mc on the right side of the brain. This facilitated comparison with previous reports of the pigeon VbC that presumed that all recordings were from the left VbC. (The projection from the IO to the VbC is exclusively contralateral.)

### Neurons selective for rotational optic flow

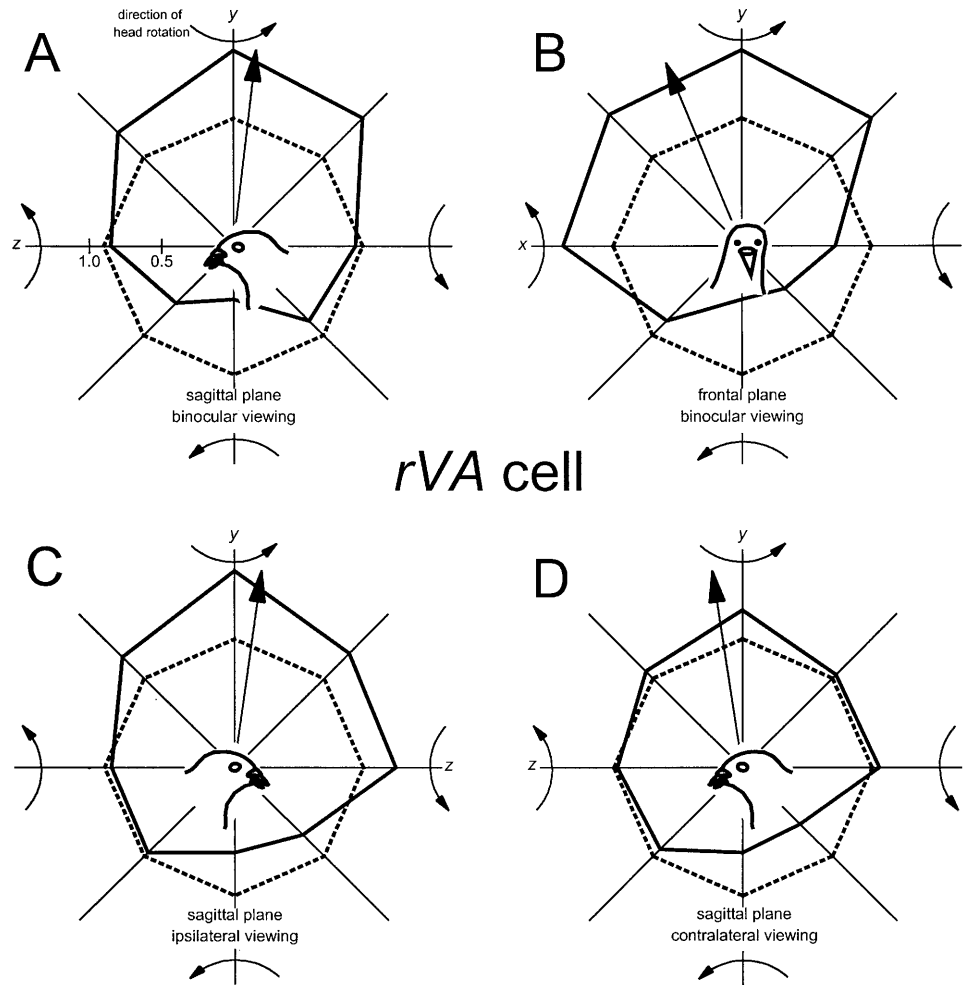
As expected from previous studies of the pigeon VbC (Wylie and Frost 1993), neurons selective for rotational optic flow could be classified into two types based on the orientation of the preferred axis: rVA neurons and rH135c neurons.

#### rVA neurons

Recordings were made from 13 rVA neurons. The direction tuning curves for an rVA neuron to sine wave gratings drifting in the frontal, ipsi- and contralateral regions of the visual field are shown in Fig. 2c. The firing rate (spikes/s relative to the spontaneous rate, SR) is plotted as a function of the direction of motion in polar coordinates. rVA neurons were excited in response to largefield stimuli moving forward (temporal-to-nasal, T-N) and backward (N-T) in the contra- and ipsilateral visual fields, respectively, and rightward motion in the frontal visual field (for neurons in the *right* IO). In the natural environment, this type of visual stimulation would occur in response to a leftward rotation of the head about the vertical (y) axis.

Figure 3 shows the responses of an rVA neuron to rotational optic flow (about several axes) produced by the planetarium projector. In Fig. 3a, an “elevation tuning curve” in the sagittal (y-z) plane is shown. The axis of the planetarium projector was placed in four orientations within the sagittal plane: the z (roll)-axis, the y (yaw)-axis and the two intermediate axes. The z- and y-axes are equivalent to  $0^\circ$  and  $90^\circ$  elevation, respectively, and the intermediate axes fall at  $+45^\circ$  and  $-45^\circ$  ( $+135^\circ$ ) elevation. The firing rate (spikes per second) of the cell in response to rotational optic flow in both directions about each of four axes is plotted in polar coordinates. For this and subsequent figures concerned with responses to rotational optic flow (Figs. 4, 5), a standard head-centric, right-handed rule is used to represent the direction of optic flow. If the thumb of the right hand is aligned with the axis, the fingers indicate the direction of head rotation. The direction of the optic flow would be opposite to the direction of head rotation. For example, the response to the leftward/rightward *head rotation* about the vertical (yaw) axis is represented by the positive/negative direction along the

**Fig. 3a–d** Responses of an rVA neuron. **a** and **b** show polar plots of elevation tuning curves in the sagittal and frontal planes, respectively, under binocular viewing conditions. **c** and **d** show elevation tuning curves in the sagittal plane under monocular viewing conditions. Firing rate (spikes per second) is plotted as a function of the orientation of the axis of rotational optic flow (solid line). Broken circles represent the spontaneous firing rate, and the solid arrows indicate the preferred axes from the best-fit cosines. A standard head-centric, right-handed rule is used to represent the direction of optic flow. Semicircular arrows represent the direction of head rotation, which is opposite the direction of optic flow. Note that this cell responded best to the flowfield that results from leftward rotation of the head about the vertical (yaw) axis (i.e. rightward optic flow: backward motion in the ipsilateral hemifield, forward motion in the contralateral hemifield). See text for a detailed description



*y*-axis. Thus, the response to the rightward/leftward *optic flow* about the *vertical* (yaw)-axis is represented by the positive/negative direction along the *y*-axis. Likewise, in the positive direction along the *z*-axis, the response to a clockwise (CW) roll of the head is represented. That, is the response to counter-clockwise (CCW) optic flow is plotted. Although redundant, semi-circular arrows on the figures explicitly illustrate the direction of head rotation for each axis. In this and subsequent polar plots, the solid arrows represents the vector of maximal excitation (“best axis”) determined from the phase of the best-fit cosine to the tuning curve. Figure 3b shows an elevation tuning curve in the frontal (*x*-*y*) plane. In Fig. 3a and b, the data were obtained with both eyes open (binocular viewing conditions). In Fig. 3c, d, elevation tuning in the sagittal plane is shown for monocular stimulation of the ipsi- and contralateral eyes, respectively. For these rVA neurons, maximal excitation was induced by the optic flowfield resulting from leftward rotation of the head about the vertical axis, and optic flow about the vertical axis in the opposite direction resulted in maximal inhibition (Fig. 3a, b). In the sagittal plane (Fig. 3a), the best axis fell approximately along the vertical axis, and rotation about the *z*-axis resulted in no modulation. In the frontal plane (Fig. 3b),

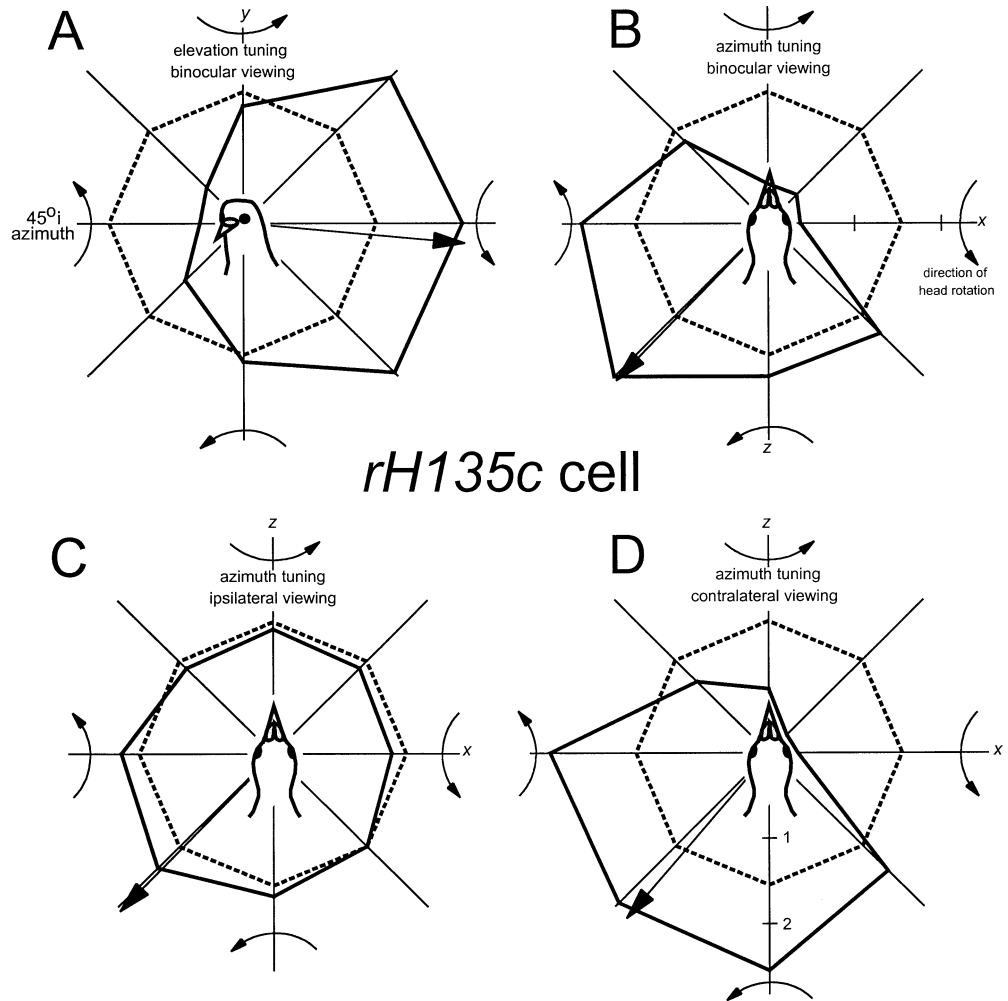
the best axis was about  $20^\circ$  from the vertical axis. With monocular stimulation, the best axes in the sagittal plane were approximately vertical for both ipsi- and contralateral stimulation. Clearly there was more modulation under binocular viewing conditions (Fig. 3a compared with c). Note that the depth of modulation was greater for stimulation of the ipsilateral eye compared with the contralateral eye (see the section Ocular dominance).

#### *rH135c neurons*

Recordings were made from 13 rH135c neurons in mc. The direction tuning curves for a rH135c neuron to sine wave gratings drifting in the frontal, ipsi- and contralateral regions of the visual field are shown in Fig. 2d. This neuron was excited in response to largefield stimuli moving upward in the contralateral and frontal visual fields, and downward motion in the ipsilateral visual field. In the natural environment, this type of visual stimulation would occur in response to rotation of the head about a horizontal axis oriented at  $135^\circ$  azimuth.

Figure 4 shows the responses of an rH135c neuron to rotational optic flow produced by the planetarium pro-

**Fig. 4a–d** Responses of an rH135c neuron. Azimuth tuning curves for binocular, ipsilateral (i) and contralateral (c) viewing conditions are illustrated in **b**, **c** and **d**, respectively. **a** shows an elevation tuning curve in a vertical plane intersecting the horizontal plane at  $45^\circ$  i azimuth. *Broken circles* represent the spontaneous firing rate, and the *solid arrows* indicate the preferred axes from the best-fit cosines. A standard head-centric, right-handed rule is used to represent the direction of optic flow. *Semicircular arrows* represent the direction of head rotation, which is opposite the direction of optic flow. This neuron responded best to rotational optic flow resulting from rotation of the head about an axis oriented in the horizontal plane at about  $135^\circ$  c azimuth. See text for a detailed description



jector. “Azimuth tuning curves” are shown in Fig. 4b–d for binocular, ipsilateral and contralateral viewing conditions, respectively. For azimuth tuning, the axis of the planetarium projector was placed in four orientations within the horizontal plane: the  $z$  (roll)-axis, the  $x$  (pitch)-axis and the two intermediate axes. The  $z$ - and  $x$ -axes are equivalent to  $0^\circ$  and  $90^\circ$  i azimuth, respectively ( $-x=90^\circ$  c azimuth). The intermediate axes fall at  $45^\circ$  i and  $45^\circ$  c azimuth. In Fig. 4a, an elevation tuning curve in a vertical plane that intersects the horizontal plane at  $45^\circ$  i azimuth is shown (binocular viewing). For this tuning curve, the axis of the planetarium projector was placed in four orientations within this plane: a horizontal axis at  $45^\circ$  i azimuth ( $0^\circ$  elevation), the  $y$  (yaw)-axis ( $90^\circ$  elevation), and two intermediate axes ( $45^\circ$  i azimuth/ $+45^\circ$  elevation and  $45^\circ$  i azimuth/ $-45^\circ$  elevation). For rH135c neurons, maximal modulation occurred in response to rotational optic flow about a horizontal axis oriented at  $135^\circ$  c azimuth (Fig. 4a, b). (From the bird’s point of view, maximal excitation occurred in response to CCW rotational optic flow about this axis, and maximal inhibition occurred in response to CW optic flow.) Little modulation occurred in response to rotation about orthogonal axes: the vertical axis (Fig. 4a) and the hori-

zontal axis through  $45^\circ$  c azimuth (Fig. 4b). The best axis for azimuth tuning was similar for stimulation of the ipsi- and contralateral eyes, but clearly there was a marked contralateral dominance.

#### *Mean best axes of rotation-sensitive neurons in IO and VbC*

Under binocular viewing conditions, elevation tuning curves in the sagittal plane were obtained for nine rVA neurons in mc and the best axes are shown in Fig. 5a. The mean of this distribution, indicated by the large broken arrow, was  $78.3^\circ$  elevation. In Fig. 5b, the distribution of the best axes of rVA neurons in the pigeon VbC are shown (from Wylie and Frost 1993). The mean of this distribution was  $89.0^\circ$ . These two distributions were significantly different ( $t$ -test;  $P<0.05$ ).

Azimuth tuning curves were obtained for ten rH135c neurons in mc under binocular viewing conditions and the best axes are shown in Fig. 5c. The mean of this distribution, indicated by the large broken arrow, was  $136.2^\circ$  c azimuth. In Fig. 5d, the distribution of the best axes of rH135i neurons in the pigeon VbC are shown

**Fig. 5a–d** Best axes of rVA and rH135c neurons in the inferior olive (IO) and vestibulocerebellum (VbC). Best axes for the elevation tuning curves (sagittal plane) of rVA neurons in IO from this study are represented by the *smaller arrows* in **a**. Best axes for the complex spike activity of rVA Purkinje cells in the flocculus of the pigeon VbC are shown in **b**. **c** and **d** show best axes from azimuth tuning curves for rH135c neurons in the IO and rH135i neurons in the flocculus of the pigeon VbC, respectively. The *larger dashed arrows* represent the means of the respective distributions. The VbC data were obtained from Wylie and Frost (1993). It is assumed that recordings were made from the right IO and left VbC as the projections from the mc of the IO to the VbC are exclusively contralateral

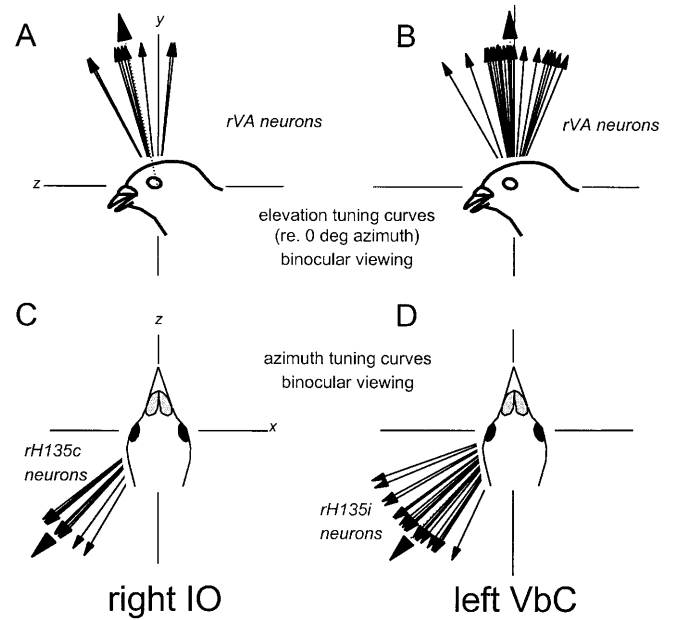


**Fig. 6a–d** Elevation tuning curves for a  $t(+y)$  neuron. **a** and **b** show elevation tuning curves in the sagittal and frontal planes, respectively, under binocular viewing conditions. Firing rate (spikes per second) in response to translational optic flowfields is plotted as a function of the orientation of the axis of translation (*solid line*). *Dashed arrows* along each axis represent the direction of self-motion the animal would make to cause the simulated flow-field (i.e. the arrows point toward the FOE in the flowfield). *Broken circles* represent the spontaneous firing rate, and the *solid arrows* indicate the axes of maximal modulation (i.e. direction of self-translation resulting in maximal modulation) from the best-fit cosines. The responses are also shown in peri-stimulus time histograms (PSTHs) for each axis. For each sweep there was 5 s of translation in one direction, followed by a 5-s pause, followed by 5-s translation in the opposite direction. The PSTHs were summed from 10 consecutive sweeps. **c** and **d** show tuning curves in the sagittal plane under monocular viewing conditions. For this cell, maximal modulation occurred in response to optic flow corresponding to upward translation (i.e. downward optic flow). See text for additional details

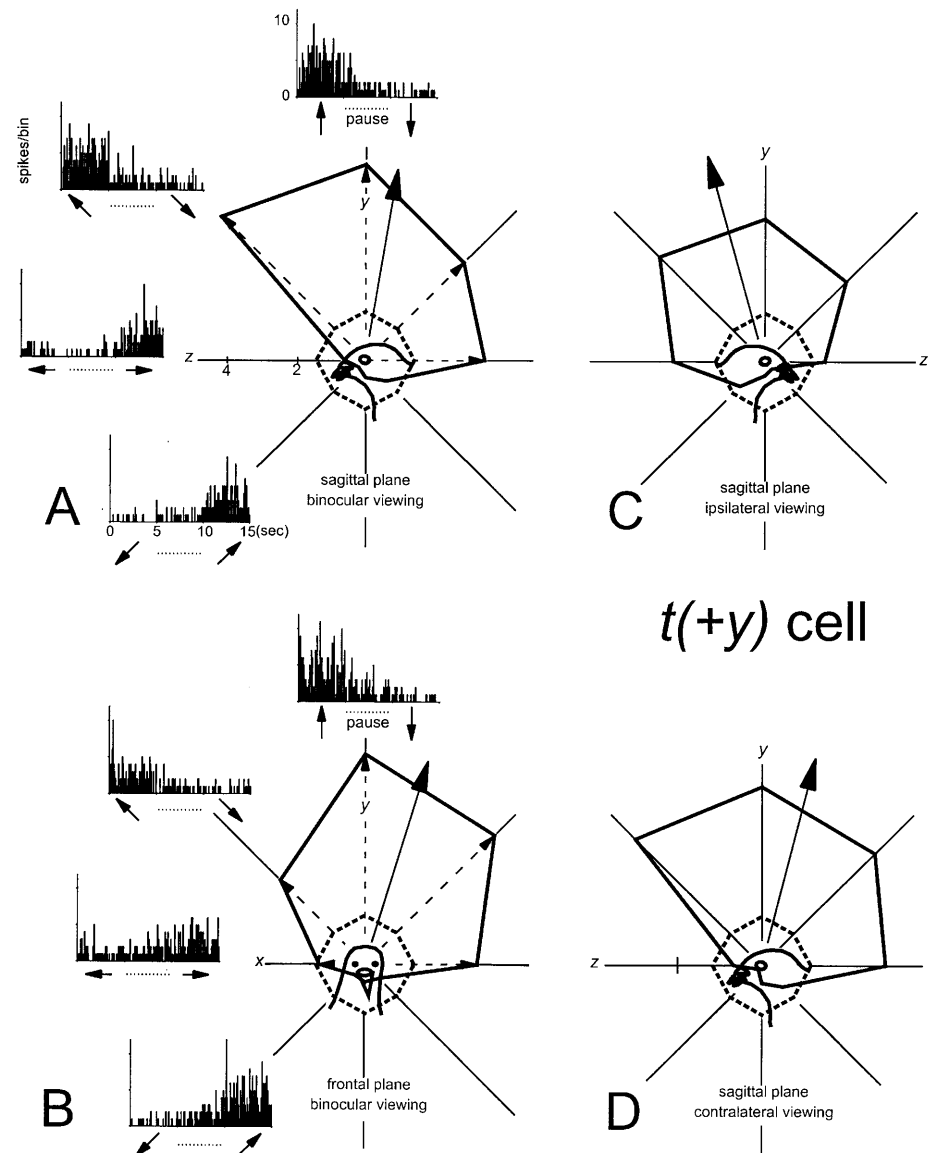
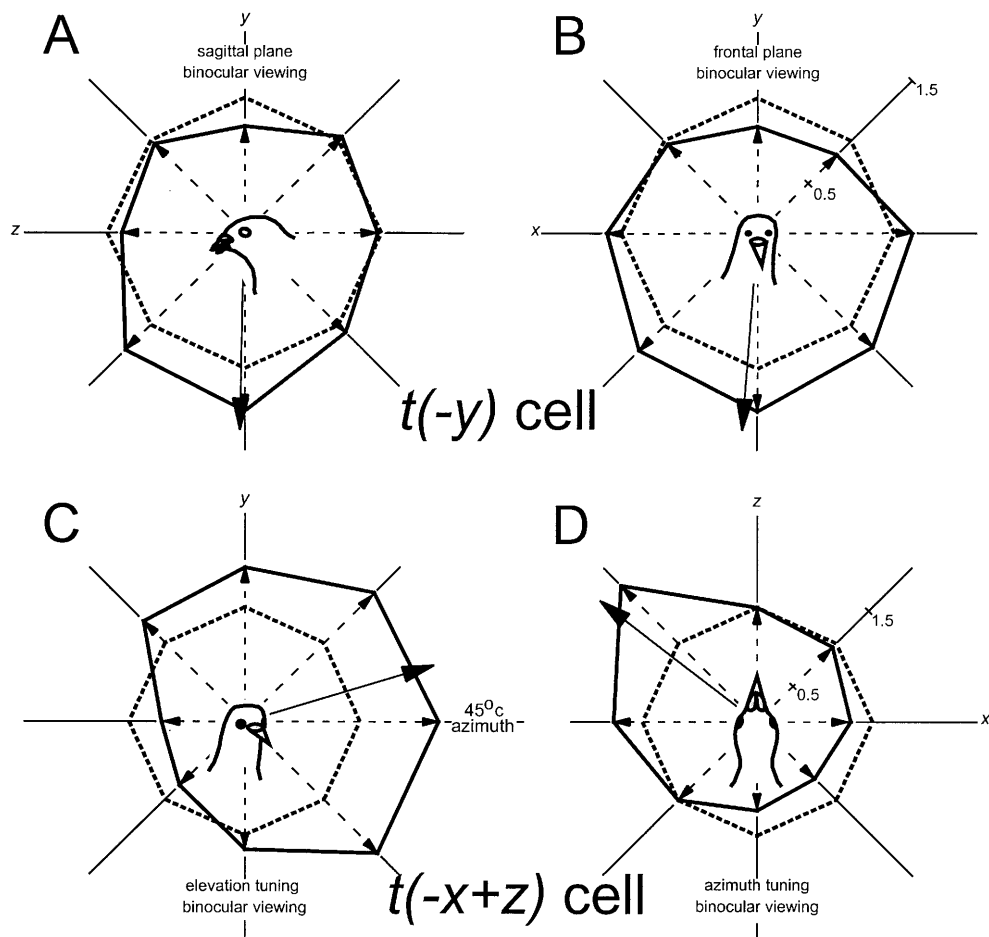


**Fig. 7a–d** Binocular tuning curves for  $t(-y)$  and  $t(-x+z)$  neurons. Elevation tuning curves for binocular viewing in the sagittal and frontal planes are shown for a  $t(-y)$  neuron in **a** and **b**, respectively. **c** and **d**, respectively, show azimuth and elevation tuning curves for a  $t(-x+z)$  neuron. *Dashed arrows* along each axis represent the direction of self-motion the animal would make to cause the simulated flowfield. *Broken circles* represent the spontaneous firing rate, and the *solid arrows* indicate the best axes from the best fit cosines. For the  $t(-y)$ , note the preference for downward translation along the  $y$ -axis (**a** and **b**, i.e. upward optic flow). For the  $t(-x+z)$  neuron, the best axis in the horizontal plane was  $52^\circ$  azimuth (**d**). The elevation tuning curve was done in the vertical plane intersecting the horizontal plane through  $45^\circ$  azimuth. The best axis was  $+16^\circ$  elevation



(mean  $135.7^\circ$  azimuth; from Wylie and Frost 1993; note that this is ipsilateral for IO neurons, contralateral for VbC neurons).

#### Neurons selective for translational optic flow

As expected from previous studies of the pigeon VbC (Wylie et al. 1998; Wylie and Frost 1999a), neurons selective for translational optic flow could be classified into four types based on the orientation of the preferred axis:  $t(+y)$ ,  $t(-y)$ ,  $t(-x-z)$  and  $t(-x+z)$  neurons.

#### $t(+y)$ neurons

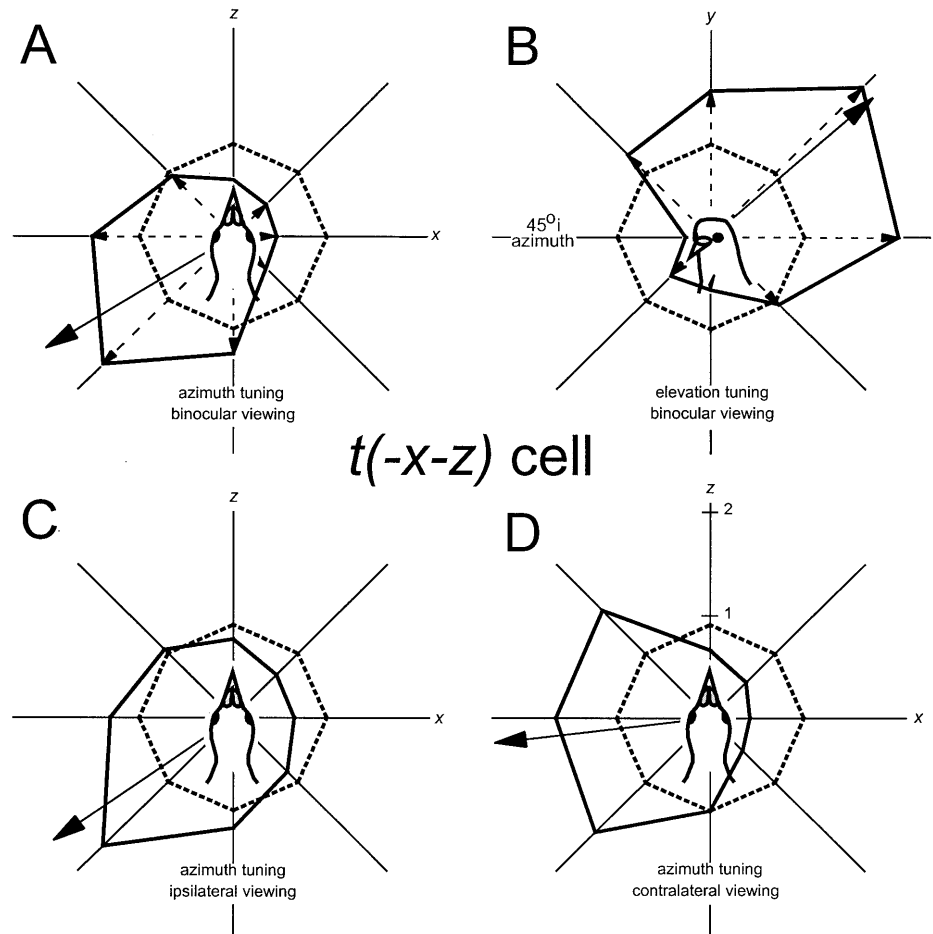
Recordings were made from eight  $t(+y)$  neurons. In response to the drifting gratings, these neurons responded best to downward motion in the ipsi-, contralateral and frontal areas of the visual field, although, for the neuron shown in Fig. 2e, there was little modulation in response to gratings in the contralateral hemifield. Figure 6 shows the responses of a  $t(+y)$  neuron to translational optic flow (produced by the translator projector) along several axes. In this figure, and subsequent figures concerning translational optic flow (Figs. 7, 8, 9), the dashed arrows along each axis represent the direction of self-motion the animal

would make to cause the simulated flowfield. That is, the arrows point toward the FOE in the flowfield. For example, an arrow pointing upward along the  $y$ -axis represents the flowfield resulting from upward self-motion: a FOE above the bird's head and downward optic flow throughout most of the visual field. Elevation tuning curves in the sagittal plane (Fig. 6a) and frontal planes (Fig. 6b) under binocular viewing conditions are shown. The maximal depth of modulation occurred in response to translational optic flow along the  $y$ -axis. Maximal excitation occurred in response to the optic flow that results from upward self-translation ( $+y$ ), i.e. downward optic flow. Elevation tuning curves in the sagittal plane are also shown for monocular stimulation of the ipsi- and contralateral eyes (Fig. 6c, d). Note that there was a greater depth of modulation in response to the stimulation of the contralateral eye.

#### $t(-y)$ neurons

Only three  $t(-y)$  neurons were encountered. In response to drifting largefield gratings, these neurons preferred upward motion in the ipsilateral, contralateral and frontal regions of the visual field (not shown). In response to panoramic flowfields produced by the translator, these neurons showed the opposite direction preference com-

**Fig. 8a-d** Axis tuning for a  $t(-x-z)$  neuron. **a** and **b**, respectively show azimuth tuning and elevation tuning (in a vertical plane intersecting the horizontal plane through  $45^\circ$  i azimuth) under binocular viewing conditions. *Dashed arrows* along each axis represent the direction of self-motion the animal would make to cause the simulated flowfield. *Broken circles* represent the spontaneous firing rate, and the *solid arrows* indicate the axes of maximal modulation from the best-fit cosines. Maximal excitation of this neuron occurs in response to an optic flowfield with FOC at  $59^\circ$  i azimuth (**a**) and  $-40^\circ$  elevation (**b**). **c** and **d** show azimuth tuning curves in the horizontal plane under monocular viewing conditions. This neuron was modulated by stimulation of both ipsilateral and contralateral eyes, but there was a disparity with respect to the best axes



pared with the  $t(+y)$  neurons. Elevation tuning curves in the sagittal and frontal planes are shown for a  $t(-y)$  neuron in Fig. 7a, b (binocular viewing).

#### $t(-x+z)$ neurons

Recordings were made from 5  $t(-x+z)$  neurons. In response to the drifting largefield gratings, these neurons responded best to backward (N-T) motion in the ipsilateral and contralateral hemifields, and rightward motion in the frontal area of the visual field (not shown). Figure 7d shows an azimuth tuning curve for a  $t(-x+z)$  neuron to translational optic flow under binocular viewing conditions. The best axis in this plane was at  $52^\circ$  c azimuth. In Fig. 7c, an elevation tuning curve in a vertical plane that intersects the horizontal plane through  $45^\circ$  c azimuth is shown for the same neuron. The best axis in this plane was located at  $+16^\circ$  elevation in this plane. That is, maximal excitation occurred in response to optic flow with a FOE at about  $52^\circ$  c azimuth/ $+16^\circ$  elevation.

#### $t(-x-z)$ neurons

Recordings were made from seven  $t(-x-z)$  neurons. In response to the drifting largefield gratings, these neurons

responded best to forward (T-N) motion in the ipsilateral and contralateral hemifields, and rightward motion in the frontal area of the visual field. This is shown in Fig. 2f, although this particular neuron showed very little modulation to stimulation of the contralateral hemi-field. Figure 8a shows an azimuth tuning curve for a  $t(-x-z)$  neuron to translational optic flow under binocular viewing conditions. The best axis in this plane was at  $121^\circ$  c azimuth. In Fig. 8b, an elevation tuning curve in a vertical plane that intersects the horizontal plane through  $45^\circ$  i azimuth is shown for the same neuron. There was a clear elevational component to the best axis for this neuron ( $+40^\circ$  elevation). That is, maximal excitation occurred in response to optic flow with a FOC at about  $59^\circ$  i azimuth/ $-40^\circ$  elevation. Figure 8c, d shows azimuth tuning curves for the neuron under monocular viewing conditions. This neuron showed substantial modulation to stimulation of both the ipsilateral and contralateral eyes, but there was a disparity with respect to the best axes.

#### Mean best axes of translation-sensitive neurons in IO and VbC

For seven  $t(+y)$  neurons, the best axes determined from elevation tuning in the sagittal plane are shown in Fig. 9a (mean  $87.6^\circ$  elevation). In Fig. 9b, the best axes of  $t(+y)$

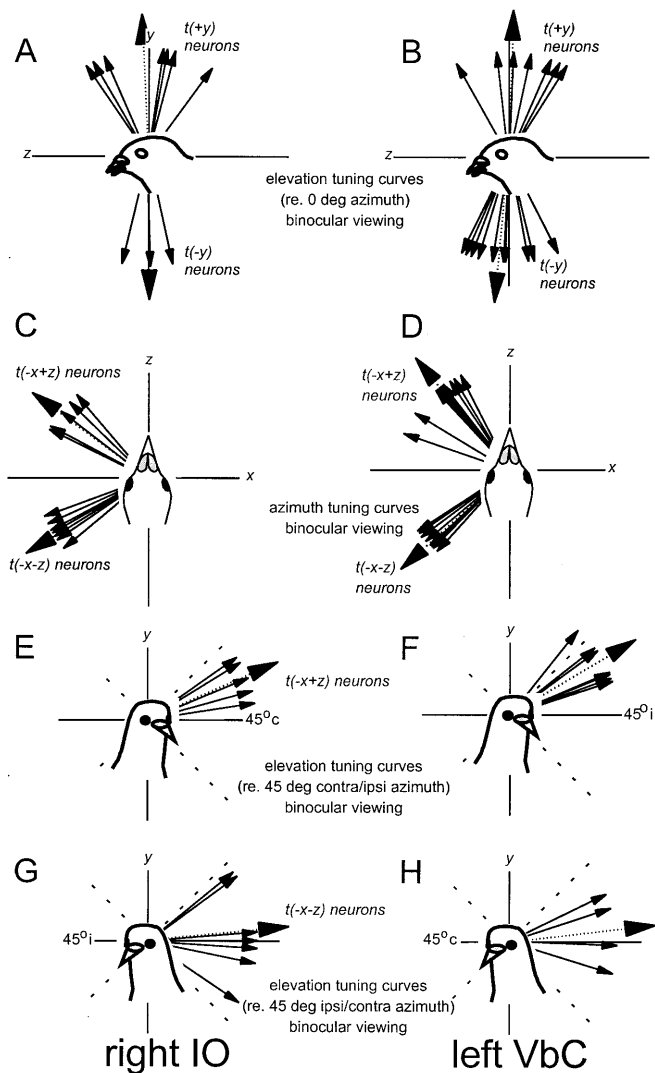


**Fig. 9a-h** Axes of maximal modulation of translation-sensitive neurons in the inferior olive (IO) and vestibulocerebellum (VbC). *Small arrows* represent best axes for individual neurons and the *larger dashed arrows* represent the means of the distributions. **a** and **b** show the best axes for elevation tuning curves in the sagittal plane for  $t(+y)$  and  $t(-y)$  neurons in the IO and VbC, respectively. **c** and **d** show the best axes for azimuth tuning curves in the horizontal plane conditions for  $t(-x+z)$  and  $t(-x-z)$  neurons in IO and VbC, respectively. **e** and **f** show the best axes from elevation tuning curves for  $t(-x+z)$  neurons in IO and VbC, respectively. Likewise, **g** and **h** show the best axes from elevation tuning curves for  $t(-x-z)$  neurons in IO and VbC, respectively. Note that best axes for  $t(-x+z)$  neurons in both IO and VbC contained a  $+y$  elevation component. The VbC data were obtained from Wylie and Frost (1999a). It is assumed that recordings were made from the right IO and left VbC

neurons from the pigeon VbC are also shown ( $91.1^\circ$  elevation; from Wylie and Frost 1999a). Also in Fig. 9a, the best axes for the three  $t(-y)$  neurons are shown (mean  $-89.5^\circ$  elevation), and in Fig. 9b the best axes of  $t(-y)$  neurons in the pigeon VbC are shown (mean  $-85.5^\circ$  elevation; from Wylie and Frost 1999a).

The best axes determined from azimuth tuning curves for the five  $t(-x+z)$  neurons in the mc, and Purkinje cells

in the VbC (from Wylie and Frost 1999a) are shown in Fig. 9c and d, respectively. The means of the distributions for  $t(-x+z)$  neurons in the mc and VbC were  $52.6^\circ$  c and  $39.7^\circ$  c azimuth, respectively, but the distributions were not significantly different (Mann-Whitney  $U$ -test). In Fig. 9e, f, the best axes from elevation tuning curves are shown for  $t(-x+z)$  neurons in the mc and VbC (from Wylie and Frost 1999a). For all neurons the best axis was located above the horizontal plane. The means for the mc and VbC distributions were  $+23.6^\circ$  and  $+29.6^\circ$  elevation, respectively.

The best axes determined from azimuth tuning curves for the seven  $t(-x-z)$  neurons in the mc and Purkinje cells in the VbC (from Wylie and Frost 1999a) are shown in Fig. 9c and d, respectively. The means of the distributions for  $t(-x-z)$  neurons in the mc and VbC were  $120.8^\circ$  c and  $133.1^\circ$  c azimuth, respectively. These distributions were significantly different ( $P < 0.002$ ; Mann-Whitney  $U$ -test). In Fig. 9g, h, the best axes from elevation tuning curves are shown for  $t(-x-z)$  neurons in the mc and VbC (from Wylie and Frost 1999a). The means for the mc and VbC distributions were  $+5.1^\circ$  and  $+6.2^\circ$  elevation, respectively.

#### Ocular dominance

Ocular dominance (OD) for each neuron was determined using the following formula:

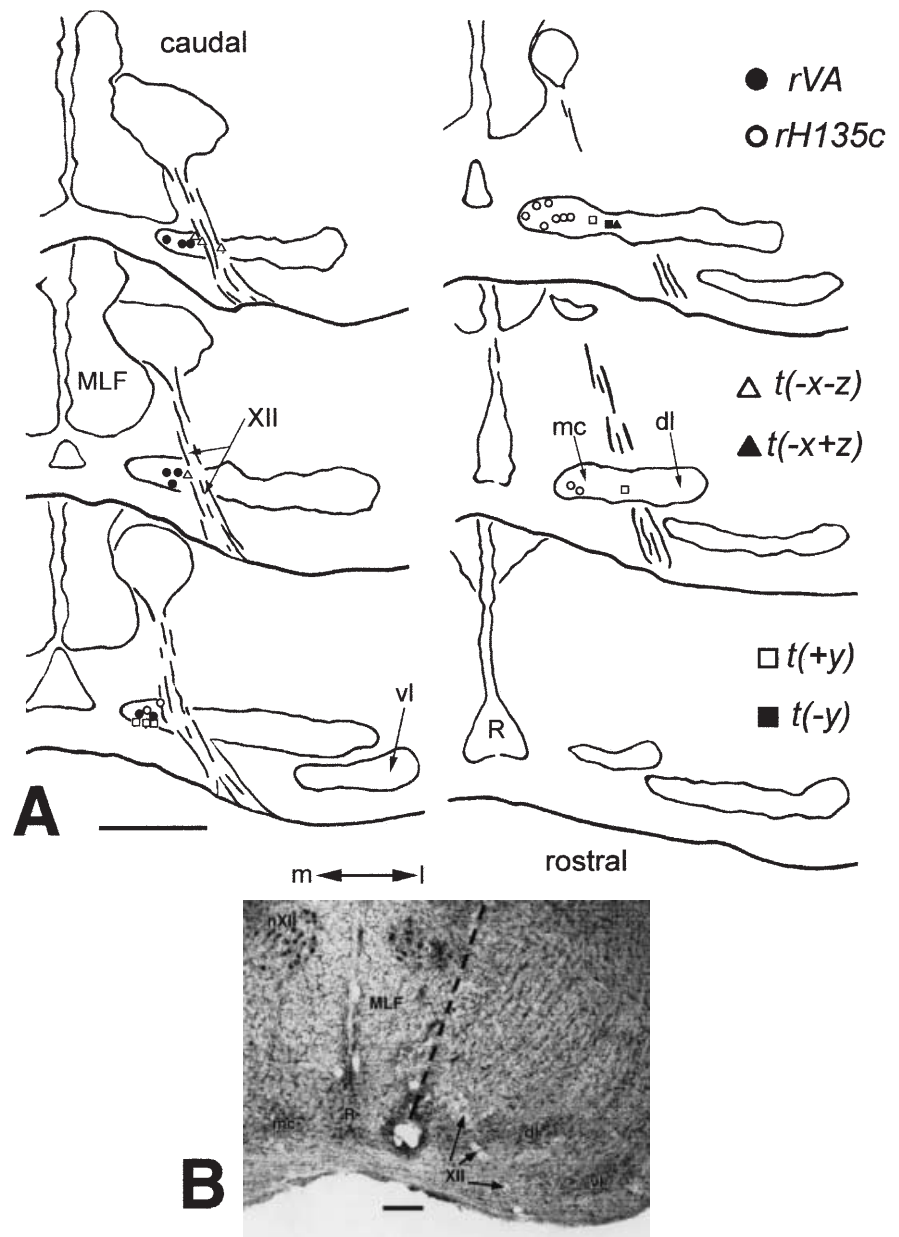
$$OD = \{(Pd - APd)/(Pnd - APnd)\}$$

where:  $P$  and  $AP$ , respectively, refer to the firing rate in response to translation/rotation optic flow moving in the preferred and anti-preferred directions along/about the best-response axis;  $d$  and  $nd$  refer to dominant and non-dominant eyes. The OD ratios were then used to categorize the neurons on a 5-point scale that we have used previously (Wylie et al. 1993). Cells were classified as markedly dominant ( $OD > 1.5$ ), slightly dominant ( $1.5 > OD > 1.1$ ) or equi-dominant ( $OD < 1.1$ ). Overall, there was a slight bias towards a contralateral dominance. Of 38 total cells, 13 showed a marked contralateral OD and 8 showed a slight contralateral OD dominance. Eight cells showed a marked ipsilateral OD, 5 showed a slight ipsilateral OD and 1 cell was monocular-ipsilateral. Three cells were equi-dominant. There were no appreciable differences among the different cell types, with the exception that seven of the nine rH135c cells showed a marked contralateral dominance.

#### Functional organization of the IO

Electrolytic lesions were made at known locations relative to neurons in the mc such that the functional organization of the mc could be assessed. Figure 10a is a series of drawings through the IO (caudal to rostral) that shows the locations of physiologically identified rotation- or translation-sensitive neurons. This included 8 rVA, 11 rH135c, 5  $t(+y)$  and 4  $t(-x-z)$  neurons. Unfortunately

**Fig. 10a, b** Functional organization of the inferior olive (IO). **a** is a series of drawings through the IO (caudal to rostral, approximately 260  $\mu$ m apart), showing the locations of physiologically identified rotation- or translation-sensitive neurons. This included 8 *rVA* (filled circles), 11 *rH135c* (empty circles), 5 *t(+y)* (empty squares), 4 *t(-x-z)* (empty triangles), 1 *t(-y)* (filled square) and 1 *t(-x+z)* (filled triangle) neuron. **b** shows a photomicrograph of a lesion in the medial column (*mc*). The dashed line indicates the electrode track. This large lesion was made at the location of an *rH135c* neuron in the most medial part of *mc*. (*MLF* medial longitudinal fasciculus, *XII* twelfth cranial nerve, *nXII* nucleus of the 12th nerve, *dl* dorsal lamella, *vl* ventral lamella, *m* medial, *l* lateral). Scale bars: **a** 500  $\mu$ m, **b** 250  $\mu$ m



there was only one each for the *t(-y)* and *t(-x+z)* groups. A clear topography is evident. The rotation cells were found medial to the translation cells, with the *rVA* neurons located caudal to the *rH135c* neurons. With respect to the translation neurons, the *t(-x-z)* neurons were found caudal to the other three types and lateral to the *rVA* neurons. Figure 10b shows a photomicrograph of a lesion in the *mc*. This lesion, which was almost twice as large as most, was made at the location of an *rH135c* neuron in the most medial part of the *mc*. This section corresponds approximately to the upper-right drawing in Fig. 10a.

## Discussion

In this study we recorded the activity of neurons in the *mc* of the IO to translational and rotational panoramic

optic flowfields produced by the planetarium and translator projectors. Six groups of neurons were found. Two groups, *rVA* and *rH135c* neurons, responded best to rotational optic flow, whereas the other four groups, *t(+y)*, *t(-y)*, *t(-x+z)* and *t(-x-z)* neurons, responded best to translational optic flow.

Comparison with studies of the pigeon VbC, nucleus of the basal optic root and pretectal nucleus lentiformis mesencephali

In pigeons, the *mc* of the IO provides CF input to all parts of the contralateral VbC, including the ventral uvula, nodulus and flocculus (Arends and Voogd 1989; Wylie et al. 1997). Previous electrophysiological studies of the pigeon VbC showed a clear functional distinction

between the lateral VbC (flocculus) and the medial VbC (ventral uvula and nodulus) with respect to the CSA of Purkinje cells in response to translational and rotational optic flow (Wylie et al. 1993). In the flocculus, two groups of rotation-sensitive neurons were found: rVA and rH135i neurons. In the medial VbC, four groups of translation-sensitive neurons were found:  $t(+y)$ ,  $t(-y)$ ,  $t(-x+z)$  and  $t(-x-z)$  neurons. As each Purkinje cell receives input from a single CF, the congruence of the findings of the present study with previous studies of the VbC is to be expected.

There were two differences from the VbC studies. First, distributions of the best axes for rVA neurons were significantly different ( $P < 0.05$ ) for the mc and VbC, although the magnitude of the difference was not striking (about  $10^\circ$ ). Upon re-examination of the VbC data (from Wylie and Frost 1993), the only other apparent difference between the two samples was that the VbC rVA neurons showed a stronger bias towards an overall ipsilateral OD and included five ipsi-monocular cells. However, OD was not correlated with the orientation of the best axis. Second, the distributions of the best axes of the  $t(-x-z)$  neurons in the mc and VbC were significantly different ( $P < 0.002$ ) and the magnitude of the difference was larger (about  $12^\circ$ ). Given the small number of neurons involved in the two samples and consequently the lack of statistical power, we are inclined to accept that these differences represent sampling error. The only methodological difference between the present study and the previous studies of the VbC was with respect to the orientation of the head during recording. In the present study, the head was oriented to the normal posture observed for running, walking and flying (Erichsen et al. 1989). For the VbC studies, the head was in the stereotaxic position; pitched down  $38^\circ$  relative to the normal position (Wylie and Frost 1993, 1999a). It is possible that otolithic inputs signalling static head tilt could account for the differences that were observed.

The mc receives visual input from two retinal-recipient nuclei: the pretectal nucleus lentiformis mesencephali (LM; Clarke 1977; Gamlin and Cohen 1988a, 1988b; Wylie 2001) and the nucleus of the basal optic root (nBOR) of the accessory optic system (AOS; Karten et al. 1977; Reiner et al. 1979; Brecha et al. 1980; Fite et al. 1981; Wylie et al. 1997; Wylie 2001). Most neurons in the LM have monocular receptive fields in the contralateral eye and respond best to moving largefield stimuli (Burns and Wallman 1981; Morgan and Frost 1981; Giovanni et al. 1984; Winterson and Brauth 1985; Wylie and Frost 1990a; Wylie and Crowder 2000). These units are the building blocks of the panoramic receptive fields in the mc and VbC that process particular patterns of optic flow resulting from self-translation and rotation. The construction of such higher-order receptive fields appears to begin before the mc. There is a small subpopulation (less than 10%) of neurons in both the nBOR and the LM that have binocular receptive fields and have a receptive field structure conducive to the detection of optic flow patterns resulting from either self-translation

or self-rotation (Wylie and Frost 1990b, 1999b; Wylie 2000). These binocular units in the nBOR appear to reside in the dorsalis subnucleus, which is the portion of the nBOR that provides most of the input to the mc (Brecha et al. 1980; Wylie 2001). However, there is clearly further integration of information from the LM and nBOR in the mc for two reasons. First, most of the binocular nBOR and LM cells show a very pronounced contralateral OD (Wylie and Frost 1990b, 1999b; Wylie 2000) compared with units in the mc and VbC (Wylie et al. 1993). Second, the best axes of these LM and nBOR units selective for either translational or rotational optic flow do not cluster as tightly about the principal axes observed for mc and VbC neurons (Wylie and Frost 1999b; Wylie 2000).

### Comparison with mammalian species

Previous studies of the IO in rabbits have found neurons responsive to rotational optic flow. Both rVA and rH135c neurons have been found in the dorsal cap (dc) of Kooy (Leonard et al. 1988). The dc provides CF input to the flocculus and to the ventral uvula and nodulus (Takeda and Maekawa 1989a, 1989b; Tan et al. 1995). Neurons responsive to translational optic flow have not been found in the IO or VbC in species other than the pigeon. However, adjacent to the dc in the beta-subnucleus of the IO, and in the medial-most zone of the nodulus and ventral uvula to which the beta-subnucleus projects, neurons are responsive to vestibular stimulation originating in the otolith organs (Barmack and Shojaku 1992, 1995). Insofar as the beta-subnucleus is potentially processing information about linear acceleration, we suggest that this structure is functionally similar to the areas of the pigeon mc that process translational optic flow.

### A common reference frame for the optokinetic, vestibular and oculomotor systems

Simpson, Graf and colleagues (Simpson and Graf 1981, 1985; Ezure and Graf 1984; Graf et al. 1988; Leonard et al. 1988; Simpson et al. 1988a, 1988b, 1989a, 1989b; van der Steen et al. 1994) have noted that the principal axes of the floccular neurons sensitive to rotational optic flow are common to the vestibular system and the extraocular muscles (for pigeons, see Baldo 1990; Wylie and Frost 1993, 1996; Dickman 1996). That is, the neural systems underlying rotational optic flow analysis, the semi-circular canals and the eye muscles, are organized with respect to a reference frame consisting of three orthogonal axes: the vertical axes and two horizontal axes oriented  $45^\circ$  to the midline. The studies of the translation-sensitive neurons in the pigeon VbC (Wylie et al. 1998; Wylie and Frost 1999a) and the present study of the mc emphasize that the translational optic flow system shares this same frame of reference: the vertical axis ( $t(-y)$  and  $t(+y)$  neurons), and two horizontal axes orient-

ed  $45^\circ$  to the midline ( $t(-x-z)$  and  $t(-x+z)$  neurons). The potential benefits and economics of such an organization have been presented in detail in previous reports (Simpson and Graf 1985; Wylie and Frost 1999a; Frost and Wylie 2000).

The principal axes of the translational optic flow system are not quite orthogonal. Although the best axes of the  $t(-x-z)$  neurons are, on average, aligned with the horizontal plane (Fig. 9g, h), this is not the case for the  $t(-x+z)$  neurons. This is clearly illustrated in Fig. 9e, f for both mc and VbC neurons. The mean of the best axes is about  $25^\circ$  above the horizontal plane. However, these results are consistent with what is known about the direction preferences of AOS neurons. Most neurons in the nBOR prefer either upward, downward or backward (N-T) largefield motion in the contralateral eye (Wylie and Frost 1990a), whereas most neurons in the LM prefer forward (T-N) motion (Winterson and Brauth 1985; Wylie and Frost 1996; Wylie and Crowder 2000). We have previously emphasized that the direction preference of N-T nBOR neurons and T-N LM neurons are not co-linear. For N-T neurons, the mean direction preference is about  $25^\circ$  down from the horizontal plane. (This is correlated with an asymmetry in the horizontal recti (see Wylie and Frost 1996 for a detailed discussion). The  $t(-x+z)$  neurons prefer N-T motion in the central areas of both hemifields. As much of the receptive field of a  $t(-x+z)$  neuron is constructed from N-T neurons in the nBOR, it is not surprising that there is an elevation component to the best axes of  $t(-x+z)$  neurons.

There remains doubt as to whether the signals from the otolith organs share the same three-axes reference frame. The primary afferents innervating the utricle in pigeons do not share this coordinate system. Si and colleagues (1997) have shown that most utricular afferents in pigeons respond best to linear translation along the interaural ( $x$ ) axis. However, Hess and Dieringer (1991) have recorded eye movements in rats to linear acceleration. Their results suggest that the otolith signals are organized in semicircular canal coordinates. Furthermore, there is evidence suggesting that the neural systems controlling postural responses to translation may be organized according to a three-axes system. In response to translation of the floor in different directions in the horizontal plane, Macpherson (1988) has found that forelimb and hind limbs of cats are maximally responsive to displacement directions approximately  $45^\circ$  to the midline.

#### Topographical organization of the mc

By making electrolytic lesions at known locations relative to recording sites, we were able to illustrate a topographical organization of the mc (Fig. 10). Previous anatomical work, using retrograde transport of cholera toxin subunit-b (CTB) from the pigeon VbC, also suggested a topographic organization of the mc. The results of the

present study are in agreement with these previous studies on several accounts. Lau et al. (1998) made large injections of CTB into the either the flocculus (rotation-sensitive cells) or medial VbC (translation-sensitive cells). From the injections into the flocculus, retrograde neurons were seen in the dorso-medial margin of the mc whereas, from injections in the medial VbC, retrograde labelling was found in the ventro-lateral mc. In the present study, the rVA and rH135c neurons were found medial to the translation-sensitive neurons.

Crowder et al. (2000) have been able to determine the projection of the mc to different classes of translation-sensitive cells by making small, iontophoretic injections of CTB into specific zones of the medial VbC. After injections into the  $t(-x-z)$  zone in the VbC, retrogradely labelled cells are found caudally in the lateral margin of the VbC. Retrograde labelled neurons from injections into the other three zones are found rostral to the  $t(-x-z)$  neurons in the mc. There is quite a bit of overlap among the locations of retrograde labelled cells from the  $t(-y)$ ,  $t(+y)$  and  $t(-x+z)$  zones, but the  $t(-y)$  neurons are found most rostrally, the  $t(-x+z)$  neurons are caudal to these, and the  $t(+y)$  neurons are found caudal and slightly medial to  $t(-x+z)$  neurons. In the present study, the  $t(-x+z)$  neurons were found caudally in the lateral mc. The  $t(-y)$ ,  $t(+y)$  and  $t(-x+z)$  neurons were found rostral to these; however, there is insufficient data to determine any segregation of these three groups.

Wylie et al. (1999) have made small, iontophoretic injections of CTB in the pigeon flocculus at locations containing either rVA or rH135i Purkinje cells. There is a clear rostro-caudal separation of the retrograde cells in the mc. After injections at locations containing rVA neurons, retrogradely labelled cells are found caudally in the medial mc. After injections at locations containing rH135i neurons, retrogradely labelled cells are found rostrally in the medial mc. In the present study, rVA cells were found in the medial mc, caudal to the rH135c cells. The organization of the rotation-sensitive cells in the rabbit IO is strikingly similar: rVA neurons are found in the caudal dc, whereas rH135c neurons are found in the rostral dc and ventro-lateral outgrowth (Leonard et al. 1988).

Recently, Wylie (2001) has shown that input to the caudal mc is mainly from the LM, whereas the nBOR provides the majority of the input to the rostral mc. (A similar pattern of connectivity to the dc has been shown in mammals; Mizuno et al. 1973; Takeda and Maekawa 1976; Maekawa and Takeda 1977; Holstege and Collewijn 1982). This is consistent with the findings of the topographical organization revealed in the present study. Recall that most LM and nBOR neurons have receptive fields restricted to the contralateral eye, and that most LM neurons prefer forward motion, whereas nBOR neurons prefer largefield stimuli moving either upwards, downwards or backwards (Burns and Wallman 1981; Morgan and Frost 1981; Gioanni et al. 1984; Winterson and Brauth 1985; Wylie and Frost 1990a, 1996; Wylie and Crowder 2000). The caudal mc contains rVA and

$t(-x-z)$  neurons. The preferred optic flowfield for both rVA and  $t(x-z)$  neurons consists of forward motion in the contralateral hemifield (e.g. Fig. 2b, e). In contrast, in the rostral mc, the preferred flowfields of rH135c,  $t(-y)$ ,  $t(+y)$  and  $t(x+z)$  neurons consist of either upwards, downwards or backwards motion in the contralateral hemifield (e.g. Fig. 2c, d). Thus, one would expect that the input to the caudal mc would be from the LM primarily, whereas the rostral mc would receive a heavier input from the nBOR.

#### Role of the rotation and translation optic flow neurons in compensatory eye and head movements

There are several mechanisms to generate compensatory eye and head movements in an attempt to stabilize the retinal image. These include optokinetic eye movements (optokinetic nystagmus, OKN), optokinetic head movements (opto-colic reflex, OCR), the vestibulo-ocular reflex (VOR) and the vestibulo-colic reflex (VCR; Wilson and Melvill Jones 1979). Pigeons exhibit robust VOR and VCR in response to head rotation (Anastasio and Correia 1988; Gioanni 1988b; Dickman et al. 2000) and robust OKN and OCR in response to rotational visual stimuli (Gioanni et al. 1981; Gioanni 1988a). The resultant head and eye movements appear to be compensatory to rotation about any axis (Gioanni 1988a; Dickman et al. 2000). The rVA and rH135c olivary cells are most certainly involved in these rotational head and eye movements. The rotational OKN and OCR are severely compromised by lesions of the nBOR and LM, the structures that are providing input to the rVA and rH135c olivary neurons (Fite et al. 1979; Gioanni et al. 1983a, 1983b). Moreover, it is thought that the olivary projection to the flocculus is involved in the adaptive modification of the rotational VOR (Ito 1972), although the role of the visual information carried by the CFs is debatable (Simpson et al. 1996). Few studies have measured compensatory eye and head movements to translation in pigeons. Dickman and Angelaki (1999) have measured the VOR (in the dark) to translation in the horizontal plane. Compensatory eye movements have not been observed, but torsional and vertical eye movements compensatory to the perceived head tilt have been observed. Given these findings, we would suggest that the translational olivary neurons do not assist the linear VOR, at least not in the way that the rotational olivary neurons assist the rotational VOR. Although it has not been demonstrated, we suggest that the translational olivary neurons are important for generating optokinetic head movement during self-translation. The stereotypical head-bobbing of pigeons is an optokinetic head movement produced during forward translation (Friedman 1975; Frost 1978).

**Acknowledgements** This research was supported by a grant from the Natural Sciences and Engineering Research Council of Canada (NSERC) to D.R.W.W. We thank X. Lu for technical assistance.

## References

- Anastasio TJ, Correia MJ (1988) A frequency and time domain study of the horizontal and vertical vestibuloocular reflex in the pigeon. *J Neurophysiol* 59:1143–1161
- Arends JJA, Voogd J (1989) Topographic aspects of the olivocerebellar system in the pigeon. *Exp Brain Res [Suppl]* 17:52–57
- Baldo MV (1990) The spatial arrangement of the semicircular canals of the pigeon. *Braz J Med Biol Res* 23:914–917
- Barmack NH, Shojaku H (1992) Vestibularly induced slow oscillations in climbing fiber responses of Purkinje cells in the cerebellar nodulus of the rabbit (letter). *Neuroscience* 50:1–5
- Barmack NH, Shojaku H (1995) Vestibular and visual climbing fiber signals evoked in the uvula-nodulus of the rabbit cerebellum by natural stimulation. *J Neurophysiol* 74:2573–2589
- Brecha N, Karten HJ, Hunt SP (1980) Projections of the nucleus of basal optic root in the pigeon: an autoradiographic and horseradish peroxidase study. *J Comp Neurol* 189:615–670
- Burns S, Wallman J (1981) Relation of single unit properties to the oculomotor function of the nucleus of the basal optic root (AOS) in chickens. *Exp Brain Res* 42:171–180
- Clarke PGH (1977) Some visual and other connections to the cerebellum of the pigeon. *J Comp Neurol* 174:535–552
- Crowder NA, Winship IR, Wylie DRW (2000) Topographic organization of inferior olive cells projecting to translational zones in the vestibulocerebellum of pigeons. *J Comp Neurol* 419:87–95
- Dickman JD (1996) Spatial orientation of semicircular canals and afferent sensitivity vectors in pigeons. *Exp Brain Res* 111:8–20
- Dickman JD, Angelaki DE (1999) Three-dimensional organization of vestibular-related eye movements to off-vertical axis rotation and linear translation in pigeons. *Exp Brain Res* 129:391–400
- Dickman JD, Beyer M, Hess BJM (2000) Three-dimensional organization of vestibular related eye movements to rotational motion in pigeons. *Vision Res* 40:2831–2844
- Erichsen JT, Hodos W, Evinger C, Bessette BB, Philips SJ (1989) Head orientation in pigeons: postural, locomotor, and visual determinants. *Brain Behav Evol* 33:268–578
- Ezure K, Graf W (1984) A quantitative analysis of the spatial organization of the vestibulo-ocular reflexes in lateral and frontal-eyed animals. I. Orientation of semicircular canals and extraocular muscles. *Neuroscience* 12:85–93
- Fite KV, Reiner T, Hunt S (1979) Optokinetic nystagmus and the accessory optic system of pigeon and turtle. *Brain Behav Evol* 16:192–202
- Fite KV, Brecha N, Karten HJ, Hunt SP (1981) Displaced ganglion cells and the accessory optic system of the pigeon. *J Comp Neurol* 195:279–288
- Friedman MB (1975) Visual control of head movements during avian locomotion. *Nature* 225:67–69
- Frost BJ (1978) The optokinetic basis of head-bobbing in the pigeon. *J Exp Biol* 74:187–195
- Frost BJ, Wylie DRW (2000) A common frame of reference for the analysis of optic flow and vestibular information. *Int Rev Neurobiol* 44:121–137
- Gamlin PDR, Cohen DH (1988a) The retinal projections to the pretectum in the pigeon (*Columba livia*). *J Comp Neurol* 269:1–17
- Gamlin PDR, Cohen DH (1988b) Projections of the retinorecipient pretectal nuclei in the pigeon (*Columba livia*). *J Comp Neurol* 269:18–46
- Gibson JJ (1954) The visual perception of objective motion and subjective movement. *Psychol Rev* 61:304–314
- Gioanni H (1988a) Stabilizing gaze reflexes in the pigeon (*Columba livia*). I. Horizontal and vertical optokinetic eye (OKN) and head (OCR) reflexes. *Exp Brain Res* 69:567–582
- Gioanni H (1988b) Stabilizing gaze reflexes in the pigeon (*Columba livia*). II. Vestibulo-ocular (VOR) and vestibulo-colic (closed loop VCR) reflexes. *Exp Brain Res* 69:583–593

- Gioanni H, Rey J, Villalobos J, Bouyer JJ, Gioanni Y (1981) Optokinetic nystagmus in the pigeon (*Columba livia*). I. Study in monocular and binocular vision. *Exp Brain Res* 44:362–370
- Gioanni H, Rey J, Villalobos J, Richard D, Dalbera A (1983a) Optokinetic nystagmus in the pigeon (*Columba livia*). II. Role of the pretectal nucleus of the accessory optic system (AOS). *Exp Brain Res* 50:237–247
- Gioanni H, Rey J, Villalobos J, Dalbera A (1983b) Optokinetic nystagmus in the pigeon (*Columba livia*). III. Role of the nucleus ectomamillaris (nEM): interactions in the accessory optic system (AOS). *Exp Brain Res* 50:248–258
- Gioanni H, Rey J, Villalobos J, Dalbera A (1984) Single unit activity in the nucleus of the basal optic root (nBOR) during optokinetic, vestibular and visuo-vestibular stimulations in the alert pigeon (*Columba livia*). *Exp Brain Res* 57:49–60
- Graf W, Simpson JI (1981) The relations between the semicircular canals, the optic axis, and the extraocular muscle in lateral-eyed and frontal-eyed animals. In: Fuchs A, Becker W (eds) *Progress in oculomotor research. (Developments in neuroscience, vol 12)* Elsevier, Amsterdam, pp 409–417
- Graf W, Simpson JI, Leonard CS (1988) Spatial organization of visual messages of the rabbit's cerebellar flocculus. II. Complex and simple spike responses of Purkinje cells. *J Neurophysiol* 60:2091–2121
- Hess BJ, Dieringer N (1991) Spatial organization of linear vestibuloocular reflexes of the rat: responses during horizontal and vertical linear acceleration. *J Neurophysiol* 66:1805–1818
- Holstege G, Collewijn H (1982) The efferent connections of the nucleus of the optic tract and the superior colliculus in rabbit. *J Comp Neurol* 209: 139–175
- Ito M (1972) Cerebellar control of the vestibular neurones: Physiology and pharmacology. *Prog Brain Res* 37:377–390
- Karten HJ, Hodos W (1967) A stereotaxic atlas of the brain of the pigeon (*Columba livia*). Johns Hopkins Press, Baltimore
- Karten HJ, Fite KV, Brecha N (1977) Specific projection of displaced retinal ganglion cells upon the accessory optic system in the pigeon (*Columba livia*). *Proc Natl Acad Sci USA* 74:1752–1756
- Lau KL, Glover RG, Linkenhoker B, Wylie DRW (1998) Topographical organization of inferior olive cells projecting to translation and rotation zones in the vestibulocerebellum of pigeons. *Neuroscience* 85:605–614
- Leonard CS, Simpson JI, Graf W (1988) Spatial organization of visual messages of the rabbit's cerebellar flocculus. I. Typology of inferior olive neurons of the dorsal cap of Kooy. *J Neurophysiol* 60:2073–2090
- Macpherson JM (1988) Strategies that simplify the control of quadrupedal stance. I. Forces at the ground. *J Neurophysiol* 60:204–217
- Maekawa K, Takeda T (1977) Afferent pathways from the visual system to the cerebellar flocculus of the rabbit. In: Baker R, Berthoz A (eds) *Control of gaze by brain stem neurons. (Developments in neuroscience, vol 1)* Elsevier, Amsterdam, pp 187–195
- Mizuno N, Mochizuki K, Akimoto C, Matsushima R (1973) Pretectal projections to the inferior olive in the rabbit. *Exp Neurol* 39:498–506
- Morgan B, Frost BJ (1981) Visual response properties of neurons in the nucleus of the basal optic root of pigeons. *Exp Brain Res* 42:184–188
- Reiner A, Brecha N, Karten HJ (1979) A specific projection of retinal displaced ganglion cells to the nucleus of the basal optic root in the chicken. *Neuroscience* 4:1679–1688
- Si X, Angelaki DE, Dickman JD (1997) Response properties of pigeon otolith afferents to linear acceleration. *Exp Brain Res* 117:242–50
- Simpson JI, Graf W (1981) Eye-muscle geometry and compensatory eye movements in lateral-eyed and frontal-eyed animals. *Ann New York Acad Sci* 374:20–30
- Simpson JI, Graf W (1985) The selection of reference frames by nature and its investigators. In: Berthoz A, Melvill-Jones G (eds) *Adaptive mechanisms in gaze control: facts and theories.* Elsevier, Amsterdam, pp 3–16
- Simpson JI, Graf W, Leonard C (1981) The coordinate system of visual climbing fibres to the flocculus. In: Fuchs AF, Becker W (eds) *Progress in oculomotor research.* Elsevier, Amsterdam, pp 475–484
- Simpson JI, Leonard CS, Soodak RE (1988a) The accessory optic system of rabbit. II. Spatial organization of direction selectivity. *J Neurophysiol* 60:2055–2072
- Simpson JI, Leonard CS, Soodak RE (1988b) The accessory optic system: analyzer of self-motion. *Ann New York Acad Sci* 545:170–179
- Simpson JI, Graf W, Leonard C (1989a) Three-dimensional representation of retinal image movement by climbing fiber activity. *Exp Brain Res [Suppl]* 17:323–327
- Simpson JI, Steen J van der, Tan J, Graf W, Leonard CS (1989b) Representations of ocular rotations in the cerebellar flocculus of the rabbit. *Prog Brain Res* 80:213–223
- Simpson JI, Wylie DR, De Zeeuw CI (1996) On climbing fiber signals and their consequence(s). *Behav Brain Sci* 19:384–398
- Steen J van der, Simpson JI, Tan J (1994) Functional and anatomic organization of three-dimensional eye movements in rabbit cerebellar flocculus. *J Neurophysiol* 72:31–46
- Takeda T, Maekawa K (1976) The origin of the pretecto-olivary tract. A study using horseradish peroxidase. *Brain Res* 117: 319–325
- Takeda T, Maekawa K (1989a) Transient direct connection of vestibular mossy fibers to the vestibulocerebellar Purkinje cells in early postnatal development of kittens. *Neuroscience* 32:99–111
- Takeda T, Maekawa K (1989b) Olivary branching projections to the flocculus, nodulus and uvula in the rabbit. II. Retrograde double labeling study with fluorescent dyes. *Exp Brain Res* 76:323–32
- Tan J, Gerrits NM, Nanhoe RS, Simpson JI, Voogd J (1995) Zonal organization of the climbing fibre projection to the flocculus and nodulus of the rabbit. A combined axonal tracing and acetylcholinesterase histochemical study. *J Comp Neurol* 356:23–50
- Wilson VJ, Melvill Jones G (1979) *Mammalian vestibular physiology.* Plenum, New York
- Winterson BJ, Brauth SE (1985) Direction-selective single units in the nucleus lentiformis mesencephali of the pigeon (*Columba livia*). *Exp Brain Res* 60:215–226
- Wylie DRW (2000) Binocular neurons in the nucleus lentiformis mesencephali in pigeons: responses to translational and rotational optic flowfields. *Neurosci Lett* 291:9–12
- Wylie DRW (2001) Projections from the nucleus of the basal optic root and nucleus lentiformis mesencephali to the inferior olive in pigeons (*Columba livia*). *J Comp Neurol* 429:502–513
- Wylie DRW, Crowder NA (2000) Spatio-temporal properties of “fast” and “slow” direction-selective neurons in the pretectal nucleus lentiformis mesencephali in pigeons. *J Neurophysiol* 84:2529–2540
- Wylie DR, Frost BJ (1990a) Visual response properties of neurons in the nucleus of the basal optic root of the pigeon: a quantitative analysis. *Exp Brain Res* 82:327–336
- Wylie DR, Frost BJ (1990b) Binocular neurons in the nucleus of the basal optic root (nBOR) of the pigeon are selective for either translational or rotational visual flow. *Vis Neurosci* 5:489–495
- Wylie DR, Frost BJ (1991) Purkinje cells in the vestibulocerebellum of the pigeon respond best to either rotational or translational visual flow. *Exp Brain Res* 86:229–232
- Wylie DR, Frost BJ (1993) Responses of pigeon vestibulocerebellar neurons to optokinetic stimulation. II. The 3-dimensional reference frame of rotation neurons in the flocculus. *J Neurophysiol* 70:2647–2659
- Wylie DRW, Frost BJ (1996) The pigeon optokinetic system: visual input in extraocular muscle coordinates. *Vis Neurosci* 13: 945–953

- Wylie DRW, Frost BJ (1999a) Complex spike activity of Purkinje cells in the ventral uvula and nodulus of pigeons in response to translational optic flowfields. *J Neurophysiol* 81:256–266
- Wylie DRW, Frost BJ (1999b) Responses of neurons in the nucleus of the basal optic root to translational and rotational flowfields. *J Neurophysiol* 81:267–276
- Wylie DR, Kripalani T-K, Frost BJ (1993) Responses of pigeon vestibulocerebellar neurons to optokinetic stimulation. I. Functional organization of neurons discriminating between translational and rotational visual flow. *J Neurophysiol* 70:2632–2646
- Wylie DRW, Linkenhoker B, Lau KL (1997) Projections of the nucleus of the basal optic root in pigeons (*Columba livia*) revealed with biotinylated dextran amine. *J Comp Neurol* 384:517–536
- Wylie DRW, Bischof WF, Frost BJ (1998) Common reference frame for the coding translational and rotational optic flow. *Nature* 392:278–282
- Wylie DRW, Winship IR, Glover RG (1999) Projections from the medial column of the inferior olive to different classes of rotation-sensitive Purkinje cells in the flocculus of pigeons. *Neurosci Lett* 268:97–100